Size Influence on the Oxygen Reduction Reaction Activity and Instability of Supported Pt Nanoparticles

Journal of The Electrochemical Society, **159** (2) B96-B103 (2012)
0013-4651/2012/159(2)/B96/8/$28.00 © The Electrochemical Society

Size Influence on the Oxygen Reduction Reaction Activity and Instability of Supported Pt Nanoparticles

Wenchao Sheng,[a] Shuo Chen,[b] Elio Vescovo,[c] and Yang Shao-Horn[b,d,*,z]

[a]*Department of Chemistry,* [b]*Department of Mechanical Engineering, and* [d]*Department of Materials Science and Engineering, Massachusetts Institute of Technology, Cambridge, Massachusetts 02139-4307, USA*
[c]*Brookhaven National Laboratory, Upton, New York 11937-5000, USA*

Size-dependent oxygen reduction reaction activity (ORR) and instability of Pt nanoparticles is of great importance in proton exchange membrane fuel cell applications. In this study, the size-dependence of ORR activity on Pt nanoparticles (NPs) was investigated on high-surface-area carbon supported Pt NPs below 5 nm in acidic electrolytes using rotating disk electrode method. The ORR activity was correlated to the estimated surface coverage by OH anion from cyclic voltammogram measurements and the surface composition and electronic structure of Pt NPs, which was studied using X-ray photoemission spectroscopy, and ultraviolet photoemission spectroscopy. The results revealed a size-independent ORR activity on Pt NPs below 5 nm, which was attributed to similar surface compositions and surface electronic structures of Pt NPs below 5 nm as well as comparable OH anion coverage at the potential where ORR was evaluated. In contrast, the instability of Pt NPs under accelerated potential cycling was found to be strongly dependent on the particle size.
 [DOI: 10.1149/2.009202jes]

Manuscript submitted August 19, 2011; revised manuscript received October 24, 2011. Published December 15, 2011.

Proton exchange membrane fuel cells (PEMFCs) show promise as a highly efficient and environmentally friendly electrochemical energy conversion technology for transport and stationary applications. The kinetics of oxygen reduction reaction (ORR)[1–3] on the cathode are sluggish, even on the most active Pt surface. Therefore, high loading of Pt in PEMFCs is required for a given power (0.2 g/kW),[1] which limits PEMFCs from large-scale commercialization. Small Pt nanoparticles (NPs) with large surface area to mass ratio are highly desirable as they provide high mass activity, where mass activity is a product of activity per surface area (specific activity, also named intrinsic activity) and surface area per mass of catalyst. With decreasing particle sizes, however, the stability of Pt NPs is reduced, which can impact the lifetime of PEMFCs.[4,5] Therefore, it is very important to elucidate the size effects on activity and stability to design Pt-based catalysts with appropriate sizes for PEMFC applications.

It has been studied intensively over the last two decades whether and how the intrinsic ORR activity of Pt NPs should be dependent on the particle size. Although it is clear that Pt NPs have reduced ORR activities compared to Pt bulk surfaces,[1,6] the influence of particle sizes on the intrinsic ORR activity in the size range relevant to practical catalysts used in PEMFCs is not well understood. Kinoshita[7] has first shown that the intrinsic ORR activity of Pt NPs drops with decreasing sizes (∼15 to ∼1.5 nm) in H_2SO_4 and H_3PO_4, and increasing surface density of under-coordinated sites and decreasing fractions of highly active Pt (100) and (111) facets, as ORR is a highly structure sensitive reaction.[8] Subsequently, the observation of decreasing ORR activity with decreasing Pt sizes from Pt polycrystalline to Pt NPs as small as 1 nm has also been made in $HClO_4$.[9,10] This trend has been attributed to increasing surface oxygenated species with decreasing coordination of surface Pt atoms on smaller Pt NPs,[9] which thus inhibits the ORR as a spectator.[11] This argument is supported by increasing OH/O adsorption strength on Pt NPs with decreasing particle sizes as revealed from X-ray photoelectron spectroscopy,[12] and X-ray absorption spectroscopy.[13] In contrast, Yano et al.[14] have found that specific ORR activity of carbon-supported Pt NPs in the range of 1 to 5 nm in 0.1 M $HClO_4$ is size-independent, which has been attributed to comparable surface electronic structure of different Pt NPs from ^{195}Pt electrochemical nuclear magnetic resonance (EC-NMR) measurements. It appears that the size effect on the intrinsic activity of Pt NPs in $HClO_4$, particularly for NP sizes equal to and smaller than 5 nm, remains inconclusive. If the specific activity is independent on Pt particle sizes, the ORR mass activity will increase on smaller Pt NPs; if the ORR specific activity decreases with decreasing particle sizes, the mass activity usually reaches a peak point at roughly $2 \sim 3$ nm,[1,15,16] probably because the enhanced electrochemical surface area (ESA) cannot fully compensate the loss of ORR specific activity on particles smaller than 2 nm.

A large number of studies[17–20] have shown that Pt NPs degrade under PEMFC operation conditions, causing effective ESA loss and limiting the durability of PEMFCs, which require lifetime of a few thousands of hours for automotive applications.[4] Previous studies[19,21–24] have shown that the stability of Pt NPs can be highly size-dependent, which can be explained by the Gibbs-Thomson relation,[19,21–24] giving rise to higher free energy for Pt NP surface by $2\gamma\Omega/R$ (γ is the surface energy of the particle, Ω is the volume per atom, and R is the radius of the particle) than that of bulk surface.[25] Thus the dilemma of keeping high mass activity (usually achieved on smaller particle sizes) and durable performance (often obtained on larger particle sizes) requires finding the compromise size for Pt NPs for PEMFC applications.

In this study, we examine the ORR activity of carbon supported Pt NPs in the particle size from 1.6 nm to 4.7 nm in $HClO_4$ and H_2SO_4 by rotating disk electrode (RDE) measurements. The intrinsic ORR activity of Pt NPs on these catalysts is then correlated to the coverage of oxygenated species deduced from cyclic voltammetry, and Pt oxidation states and valence band information of Pt NPs obtained from X-ray photoemission spectroscopy and ultraviolet photoemission spectroscopy measurements. In addition, the stability of these catalysts as a function of Pt NP size was examined by potential cycling at 80 °C in H_2SO_4. The origin in the size influence on the ORR activity and instability of Pt NPs having sizes smaller than ∼5 nm is discussed.

Experimental

Physical characterization of Pt NP catalysts.— Five samples of Pt catalysts supported on high-surface-area carbon (HSAC) (Pt/C) were investigated in our study to explore the size-dependent behavior of the ORR. Three pristine Pt/C catalysts supplied by Tanaka Kikinzoku (TKK) have Pt weight fractions of 9% (TEC10E10A), 19% (TEC10E20A) and 46% (TEC1050E), respectively. The Pt/C catalyst containing 46% Pt NPs was further treated in Ar (99.999%, Airgas) at 900 °C for one minute or two hours (the ramping rate was ∼30 °C per minute) to create larger Pt particle sizes. The samples were referred to as Pt-9%, Pt-19%, Pt-46%, Pt-46%-900 °C-1m and Pt-46%-900 °C-2h in the following text. The catalysts were analyzed as-received or as-prepared with physical characterization without any further pre-treatment.

* Electrochemical Society Active Member.
z E-mail: shaohorn@mit.edu

High resolution transmission electron microscopy (HRTEM) measurements.— The Pt NP sizes of these samples were examined by a JEOL 2010 F high-resolution transmission electron microscope (HRTEM) operated at 200 kV with a point-to-point resolution of 0.19 nm. TEM samples were prepared by drop-casting the catalyst powders ultrasonicated for five minutes in ethanol onto TEM grids (Lacey carbon coated copper grids, Electron Microscopy Sciences) and then dried in air. Pt NP diameters (d) were measured from bright field TEM micrographs. The number-averaged ($d_n = \sum_1^n d_i/n$) diameter and the volume/area-averaged diameters, defined as $d_{v/a} = \sum_1^n d_i^3/\sum_1^n d_i^2$ were calculated.[4]

Ultraviolet photoemission spectroscopy measurements.— Surface electronic structures of three Pt/C catalysts (Pt-19%, Pt-46% and Pt-46%-900 °C-1m) and HSAC (TKK) were examined by ultraviolet photoemission spectroscopy (UPS), and compared with Pt foil. Pt valence band of Pt-9% were not resolved because of the low signal to noise ratio at extremely low Pt loading. The catalyst powder samples were deposited on freshly cleaved highly oriented pyrolytic graphite (HOPG, SPI Supplies). UPS measurements were performed at the U5UA beam line at the National Synchrotron Light Source at the Brookhaven National Laboratory. The ultraviolet photoemission spectra were collected with a 125-mm hemispherical analyzer at photon energies of 80 eV under ultra-high vacuum conditions of 5×10^{-11} torr. The total instrument resolution was set to 0.10 eV. As the photoemission cross section of Pt is dominated by the d states at a photon energy of 80 eV,[26] the valence band structure measured mostly reflects the valence d states. Shirley-type background was subtracted to remove the secondary electron scattering as described in the literature.[27] To obtain the photoemission contribution from Pt NPs only, the density of states of carbon was subtracted from those of Pt/C samples, following the method developed by Eberhardt et al.[28] The d band center energy relative to the Fermi level was calculated from the density of states based on $d_{center} = \int N(\varepsilon)\varepsilon d\varepsilon / \int N(\varepsilon) d\varepsilon$,[27] where N is the density of states and ε is the energy of states.

X-ray photoemission spectroscopy measurements.— Oxidation of supported Pt NPs was investigated by X-ray photoemission spectroscopy (XPS) on a Kratos Axis Ultra Spectrometer (Manchester, UK) with a monochromatized Al X-ray source (Al Kα). The minimum analysis area was set to be about 1.1 mm in diameter. Survey spectra were initially collected at low-resolution, and high-resolution spectra were collected for quantitative analysis of Pt NP composition. All spectra were calibrated with the sp^2 hybridized carbon component of C 1s at 284.5 eV.[29] The relative sensitivity factors for Pt 4f, C 1s, N 1s and O 1s were given as 5.575, 0.278, 0.477 and 0.787, respectively. After a Shirley-type background subtraction, the asymmetric photoemission spectra of Pt 4f were fitted into three species according to previous studies,[30,31] including Pt^0, Pt (II) and Pt (IV). The doublet separation between $Pt_{5/2}$ and $Pt_{7/2}$ was constrained to be 3.4±0.1 eV. The peak area between $Pt_{5/2}$ and $Pt_{7/2}$ was constrained to be roughly 3:4. The ratios between Pt species of different oxidation states were calculated from the peak areas of deconvoluted Pt 4f spectra.

Electrochemical measurements.— Preparation of Pt catalyst electrodes.— Pt loadings of ∼6.4−7.4 $\mu g_{Pt}/cm^2$ (except for 14 $\mu g_{Pt}/cm^2$for Pt-46%-900 °C-2h) on glassy carbon electrode (GCE, 5 mm in diameter, Pine Instrument) without any Nafion were used for cyclic voltammetry and ORR measurements in both $HClO_4$ and H_2SO_4. Suspensions of Pt-9%, Pt-19%, Pt-46%, Pt-46%-900 °C-1m and Pt-46%-900 °C-2h of 0.15−0.70 mg/mL were obtained by dispersing the catalysts in de-ionized water (18.2 MΩ•cm, Millipore) using ultrasonication in ice-bath. 20 μL of the Pt/C catalyst suspension was deposited on the GCE, which was pre-polished using alumina of 0.05 micron and dried in air at room temperature. Pt loadings of ∼10 $\mu g_{Pt}/cm^2$ were used for potential cycling experiments of Pt/C catalysts (Pt-46%, Pt-46%-900 °C-1m and Pt-46%-900 °C-2h), where 20 μL of 0.025 wt % Nafion water solution (diluted from 5 wt% Nafion, Ion Power, Inc.) was added to dried catalyst thin film on GCE and dried subsequently in air.

Electrochemical surface area measurements from cyclic voltammetry.— Cyclic voltammograms (CV) on Pt/C were collected in both 0.1 M $HClO_4$ (diluted from 70% $HClO_4$, GFS Chemicals) and 0.5 M H_2SO_4 (diluted from 18 M H_2SO_4, Sigma Aldrich). A Pt wire and a saturated calomel electrode (SCE, Analytical Sensor, Inc.) were employed as the counter and the reference electrode, respectively. However, all the potentials reported in this paper were referenced to that of the reversible hydrogen electrode (RHE), which was calibrated from the RDE measurements of hydrogen oxidation.[32] After the electrolyte was saturated with Ar, the steady-state CV of the working electrode was recorded at 50 mV/s from 0.03 V to 1.1 V vs. RHE at room temperature (296 ± 2 K) after it was scanned under the same condition for ∼20 cycles. CVs of catalyst thin films without Nafion binder were measured with rotation at 1600 rpm to ensure that no catalyst fell off from GCE, where no change in the CV data was found before and after rotation. The ESA of Pt/C was determined from the Pt-hydrogen desorption region between 0.05 V and ∼0.4 V (the onset of the double layer region) vs. RHE, assuming a surface charge density of 210 $\mu C/cm^2{}_{Pt}$ for a monolayer adsorption of hydrogen on Pt surface.[33]

ORR activity measurements using rotating disk electrode.— ORR activities of these Pt/C catalysts were examined in 0.1 M $HClO_4$ and 0.5 M H_2SO_4 using RDE measurements. After the electrolyte was purged with pure O_2 (99.995%, Airgas) for at least half an hour, polarization curves were recorded between ∼0.03 V and ∼1.1 V vs. RHE at a sweep rate of 10 mV/s and rotation speeds of 100, 400, 900 and 1600 rpm at room temperature. To remove the capacitive currents of these Pt/C samples, oxygen reduction currents collected in O_2 atmosphere were obtained from subtracting the polarization curve in O_2 by the corresponding CV in Ar at the same sweep rate. The kinetic current i_k was calculated based on the Koutecky-Levich equation, $1/i = 1/i_k + 1/i_D$ where i is the measured current and i_D is the mass-transport limited current. The specific activity i_s of ORR was then obtained by normalization of i_k by the ESA of Pt. i_s and the mass activity i_m (i_k normalized by the weight of Pt) at 0.9 V vs. RHE were used to compare the catalytic properties among the samples. The standard deviations were constructed from at least four repeats of experiments. The Koutecky-Levich plot, $1/i \propto 1/\omega^{1/2}$, was obtained at 0.6 V vs. RHE for $HClO_4$ and 0.4 V vs. RHE for H_2SO_4, based on $1/i = 1/i_k + 1/i_D = 1/i_k + 1/Bc_0\omega^{1/2}$. Bc_0, determined from the slope, reflects the number of electrons transferred in the reaction, and the predicted value for Bc_0 is calculated based on $i_D = 0.2nFC_{O_2}(D_{O_2})^{2/3}\nu^{-1/6}\omega^{1/2}$ [34] where n is the number of transferred electrons, F is the Faraday constant, C_{O_2} is the concentration of dissolved O_2, D_{O_2} is the diffusivity of O_2, ν is the kinetic viscosity of the electrolyte and ω is the rotation rate.[34]

Pt/C instability upon potential cycling.— Accelerated instability measurements of Pt/C catalysts were performed in N_2/Ar-saturated 0.5 M H_2SO_4 using potential cycling from 0.6 V to 1.0 V vs. RHE at 20 mV/s at 80 °C. At the beginning of each potential cycling experiment, the working electrode was scanned between ∼0.03 V and ∼1.1 V vs. RHE at a sweep rate of 200 mV/s for 60 cycles to reach steady-state CV at room temperature. The electrochemical cell was then heated up to 80 °C in an oil bath, and the working electrode was scanned between 0.6 V and 1.0 V vs. RHE at 20 mV/s. After every 200 cycles at 80 °C, the cell was cooled down to room temperature and steady-state CVs were recorded at 50 mV/s from 0.03 V to 1.1 V vs. RHE, from which the ESA of Pt/C catalysts was obtained as a function of number of cycles.

Results and Discussion

Size distributions and surface atomic structures of Pt/C catalysts.— Figure 1a−1e shows representative HRTEM images of supported Pt NPs of five catalyst samples used in this study, where single-crystalline Pt NPs were found to uniformly distribute on carbon support. For each sample, 200 particles were measured to calculate the average particle size. The pristine Pt-9%, Pt-19% and Pt-46% catalysts have a number-averaged particle size of 1.6 ± 0.5 nm,

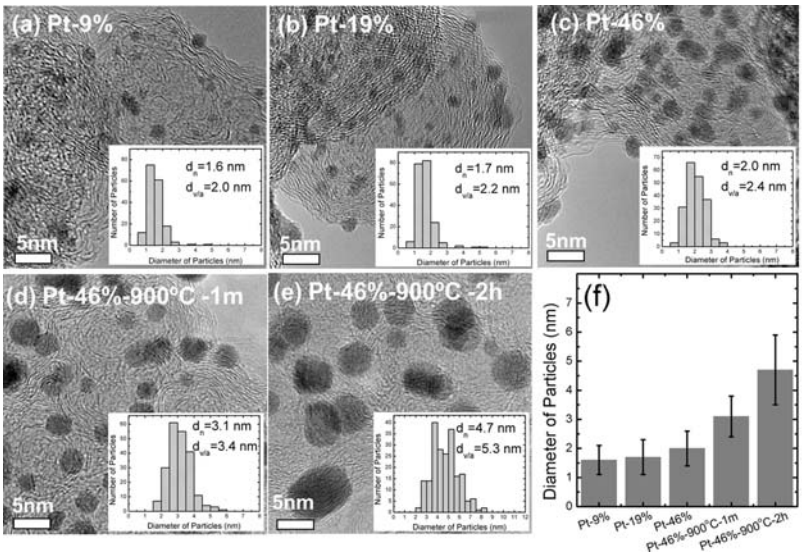

Figure 1. HRTEM images of Pt NPs for (a): Pt-9%; (b): Pt-19%; (c): Pt-46%; (d): Pt-46%-900 °C-1m; and (e): Pt-46%-900 °C-2h. (f): number-averaged diameters of Pt NPs for each sample. The scale bars are 5 nm. The insets are the Pt particle size distributions, number-averaged (d_n), and volume/area-averaged ($d_{v/a}$) particle sizes. The error bars in (f) are standard deviations of the particle size based on at least 200 counts for each sample.

1.7 ± 0.6 nm and 2.0 ± 0.6 nm, respectively, where the error bars correspond to the standard deviation of each size distribution. As shown in Figure 1f, Pt-46%-900 °C-1m and Pt-46%-900 °C-2h have larger particle sizes and wider size distributions of 3.1 ± 0.7 nm and 4.7 ± 1.2 nm, respectively.

The volume/area-averaged diameter ($d_{v/a}$) of each sample and the specific surface area (S^{TEM}) based on $d_{v/a}$ are listed in Table S1. Further investigation of Pt surface morphology was performed on samples Pt-46%, Pt-46%-900 °C-1m, and Pt-46%-900 °C-2h. As shown in Figure S1. Pt NP surfaces are found to be dominantly enclosed by Pt(111) planes, which accounts for 55%−65% of the total surfaces (Figure S1c). These three samples also have minor fraction (∼15% to 25%) of high-index planes, with the fraction slightly increased as the particle size decreases, as shown in Figure S1d. For Pt-9% and Pt-19% samples, the majority are below 2 nm in diameter. However, the conventional HRTEM is not able to well resolve the surface crystal structure of these small particles due to the strong influence from the carbon substrate, as shown in Figure S2, and thus the surface atomic structure information was not available for Pt-9% and Pt-19% samples.

Size-dependent oxidation and electronic structure of Pt NPs.— XPS was used to determine the Pt oxidation state of Pt NPs. We first compared Pt 4f and C 1s raw data of Pt-46%, Pt-46%-900 °C-1m, and Pt-46%-900 °C-2h before calibrating with the sp^2 hybridized carbon component of C 1s at 284.5 eV. The C 1s peaks were found to fluctuate between 284.4 and 284.5 eV. We did not observe a positive shift in Pt 4f or a negative shift in C 1s expected for Pt carbides, which would result from the charge transfer from Pt to C if Pt carbides would form during heat-treatment as suggested by previous studies.[35,36] Further analysis was carried out after calibrating with the sp^2 hybridized C 1s at 284.5 eV. Pt $4f_{5/2}$ and $4f_{7/2}$ profiles of these five Pt/C samples were fitted to three components: Pt^0, Pt (II) and Pt (IV) species with peak separation and peak ratio constrained, as shown in Figure S3 and Table S2. Representative Pt 4f doublet profile of the 2.0 ± 0.6 nm sample is shown in Figure 2a, having Pt^0 with Pt $4f_{7/2}$ peak at ∼71.6 eV, Pt (II) with Pt $4f_{7/2}$ peak at ∼72.9 eV, and Pt (IV) with Pt $4f_{7/2}$ at ∼74.3 eV, which are in reasonably good agreement with previous reports.[30,31] The fraction of Pt^0 was found to increase from 65% to 91% with increasing particle size from 1.6 ± 0.5 nm to 3.1 ± 0.7 nm, and eventually level off at 4.7 ± 1.2 nm, as shown in Figure 2b. The composition of Pt (IV) also disappears with these two large particle sizes. This slight size-dependent oxidation can be attributed to increased under-coordinated sites on smaller particles, which can bind more strongly with oxygen-containing species than terrace sites.[37]

Surface electronic structures of these Pt NPs were examined using UPS. Figure 3a shows the partial valence band of bare HSAC and HSAC-supported Pt NPs. The sole photoemission contributions of Pt NPs were obtained by subtracting the spectrum of HSAC from that

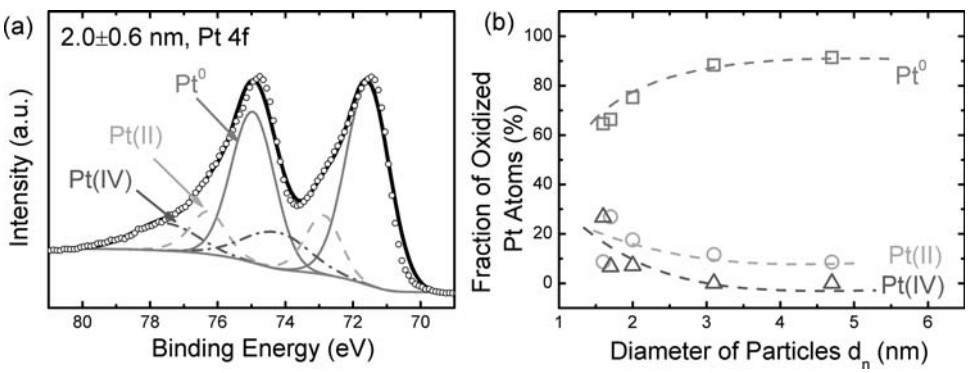

Figure 2. (a): Representative X-ray photoemission spectra of Pt 4f level for Pt-46% (2.0 ± 0.6 nm) sample. Curve fitting was done after a Shirley-type background subtraction. The Pt 4f peaks were fitted into three sets of Pt species, i.e. Pt^0 (solid red line), Pt(II) (dashed green line) and Pt(IV) (dash-dotted blue line). The doublet separation between $Pt_{5/2}$ and $Pt_{7/2}$ was constrained to be 3.4 ± 0.1 eV. The peak area ratio between $Pt_{5/2}$ and $Pt_{7/2}$ was constrained to be roughly 3:4. (b): The fractions of Pt atoms at different oxidation states calculated from the corresponding peak areas of Pt 4f spectra.

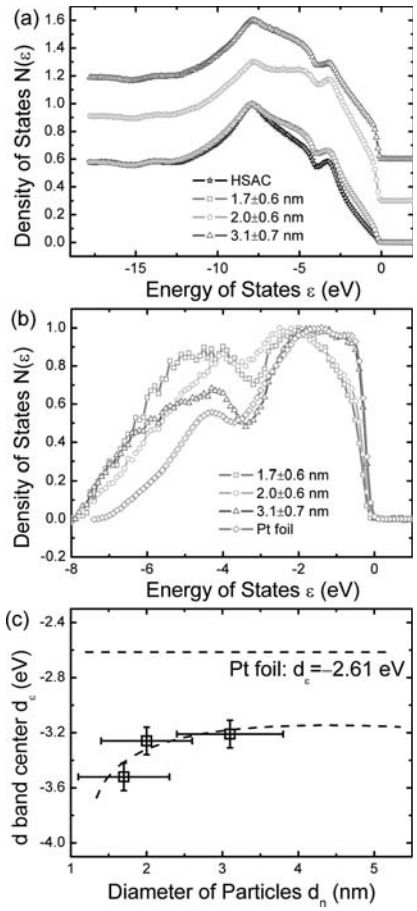

Figure 3. (a): Outer-level photoemission spectra of Pt-19% (1.7 ± 0.6 nm, red square), Pt-46% (2.0 ± 0.6 nm, green circle), Pt-46%-900 °C-1m (3.1 ± 0.7 nm, blue triangle), and a HSAC sample (black star) collected at a photon energy of 80 eV; (b): subtracted photoemission signals of Pt NPs and Pt foil (grey pentagon); and (c): the estimated d band center of Pt 5d emission relative to the Fermi level of different sized samples based on $d_{center} = \int N(\varepsilon)\varepsilon d\varepsilon / \int N(\varepsilon) d\varepsilon$.[27] The error bars of x-axis in (c) are standard deviations of Pt NPs based on at least 200 particle counts for each sample, and the error bars of y-axis in (c) are the total UPS instrumental resolution (0.1 eV).

of Pt/C, as shown in Figure 3b. While Pt NPs of 3.1 nm and Pt foil show well-developed density of states (DOS) near the Fermi level (binding energy equal to 0), Pt NPs of 1.7 nm and 2.0 nm illustrate somewhat lower DOS, probably due to the presence of ultra-small Pt NPs (<0.5 nm), the valence band of which may not have been fully developed.[38,39] However, all NP samples show higher DOS from –4 to –8 eV below the Fermi level than Pt foil. The valence band structure measured mostly reflects the valence d states because the cross section of s and p states is much smaller than that of d states at 80 eV.[26] It was found that Pt NPs have a much lower d band center compared to Pt foil, and interestingly the d band center was reduced slightly with decreasing particle size, as shown in Figure 3c. Although larger fractions of low-coordinated surface atoms[7] on Pt NPs than bulk surface should lead to a narrowed and up-shifted d band from previous DFT studies,[40–42] surface oxygen on Pt NPs can cause d band broadening and thus lower the d band center.[43] Therefore, the d-band lowering of smaller Pt NPs shown in UPS data can be attributed to increasing surface oxygenated species on Pt NPs with decreasing size as revealed by XPS results (Figure 2). This is in agreement with previous findings[44] that the d band center relative to the Fermi level of supported Pt NPs is lowered with increasing surface steps, which can bind more strongly with oxygenated species than low-index terrace sites.

ESA estimation of Pt/C catalysts.— Figures 4a and 4c show CVs of these five catalyst samples collected in Ar-saturated 0.1 M $HClO_4$ and 0.5 M H_2SO_4. The CVs of these catalysts clearly show underpotential deposition of hydrogen on Pt between 0.05 V and ~0.4 V, followed by a double layer region, and Pt-OH formation and reduction in the voltage range from 0.6 to 0.8V vs. RHE, which is in good agreement with previous studies.[10,33,45] The peaks between 0.1 and 0.2 V and the broad shoulder in between 0.2 and 0.3 V correspond to the Pt-H adsorption/desorption on Pt (110) and Pt (100) facets, respectively. The ESA of Pt/C catalysts, estimated from the charge in the hydrogen desorption region, are compared with those calculated from the HRTEM data (S^{TEM}) in Table S1. The ESA values obtained in $HClO_4$ and H_2SO_4 are very comparable, which suggests that anion adsorption may not interfere with H underpotential deposition on Pt. In $HClO_4$, Pt NPs in pristine catalysts Pt-9%, Pt-19% and Pt-46% have relatively large ESA values of 148 m^2/g_{Pt}, 126 m^2/g_{Pt}, and 78 m^2/g_{Pt}, respectively. After one minute heat treatment at 900 °C, the ESA of Pt-46% drops to 38 m^2/g_{Pt}, and it further decreases to 24 m^2/g_{Pt} after a two-hour heat treatment at 900 °C. For all samples, the ESA decreases with the increased average particle size measured from HRTEM micrographs. The HRTEM estimated surface areas (S^{TEM}) agree well with the ESAs for Pt-9% and Pt-19%, but are much larger than those of the pristine and heat treated Pt-46% samples. It is worth pointing out that the former case is likely coincident but the latter one may reflect the true differences intrinsic to these two methods in estimating Pt NP surface area. On one hand, because the contact area between Pt NPs and the carbon support is included in S^{TEM} but is inaccessible in CVs, S^{TEM} is expected to be larger than ESA. On the other hand, due to the difficulty of detecting extremely small (<0.5 nm)[32] but electrochemically active particles with conventional HRTEM, the S^{TEM} of catalyst samples with these very small Pt NPs such as Pt-9% and Pt-19% is underestimated and is expected to be smaller than ESA. Both effects may render a coincidental agreement between S^{TEM} and ESA for Pt-9% and Pt-19%. As the number of Pt NPs smaller than 0.5 nm is smaller in Pt-46% than in Pt-9% and Pt-19%, which is further reduced significantly via the heat-treatment,[5] the first effect will dominate and thus lead to greater S^{TEM} than ESA as observed.

Size-independent surface coverage of oxygenated species on Pt NPs from CV measurements.— Increasing oxidation current with an onset voltage at ~0.7 V in the positive-going scan is associated with the formation of oxygenated species on Pt (e.g. OH_{ad}) while the reduction peak around 0.6~0.8 V in the negative-going scan is related to the reduction of Pt oxides as shown in Figures 4a and 4c. The onset voltage for the formation of oxygenated species on Pt NPs was influenced by anion adsorption, where it was delayed from ~0.7 V in $HClO_4$ to ~0.8 V in H_2SO_4 in the positive-going sweep due to strong (bi)sulfate anion adsorption.[8] This effect can be seen more clearly in the charge density of oxygenated species on Pt NPs in Figures 4b and 4d (top panels), which will be discussed in detail below. For example, the charge density of 50 $\mu C/cm^2_{Pt}$ was obtained at 0.85 V in $HClO_4$ while this was achieved at 0.95 V in H_2SO_4.

With decreasing Pt particle sizes, the onset voltage of rising oxidation current and the peak voltage of the reduction peak are shifted negatively as shown in Figures 4a and 4c. To examine this further, the charge densities associated with the formation and reduction of Pt oxygenated species were calculated from CV data, as shown in Figures 4b and 4d. It is interesting to note that the coverage of oxygenated species at 0.9 V in the positive-going sweep, where ORR activity is typically evaluated, has very weak dependence on particle size in $HClO_4$ and H_2SO_4, as shown in Figures 4b and 4d (top panels) and Figure 4e. In contrast, the particle-size dependent coverage is more apparent for reduction of Pt oxygenated species on the negative-going scan (Figures 4b and 4d, bottom panels), which is in good agreement with those reported previously.[46] The particle-size-dependent reduction of Pt oxygenated species has been attributed to increasing oxyphilicity of smaller Pt NPs having decreased surface coordination, and the

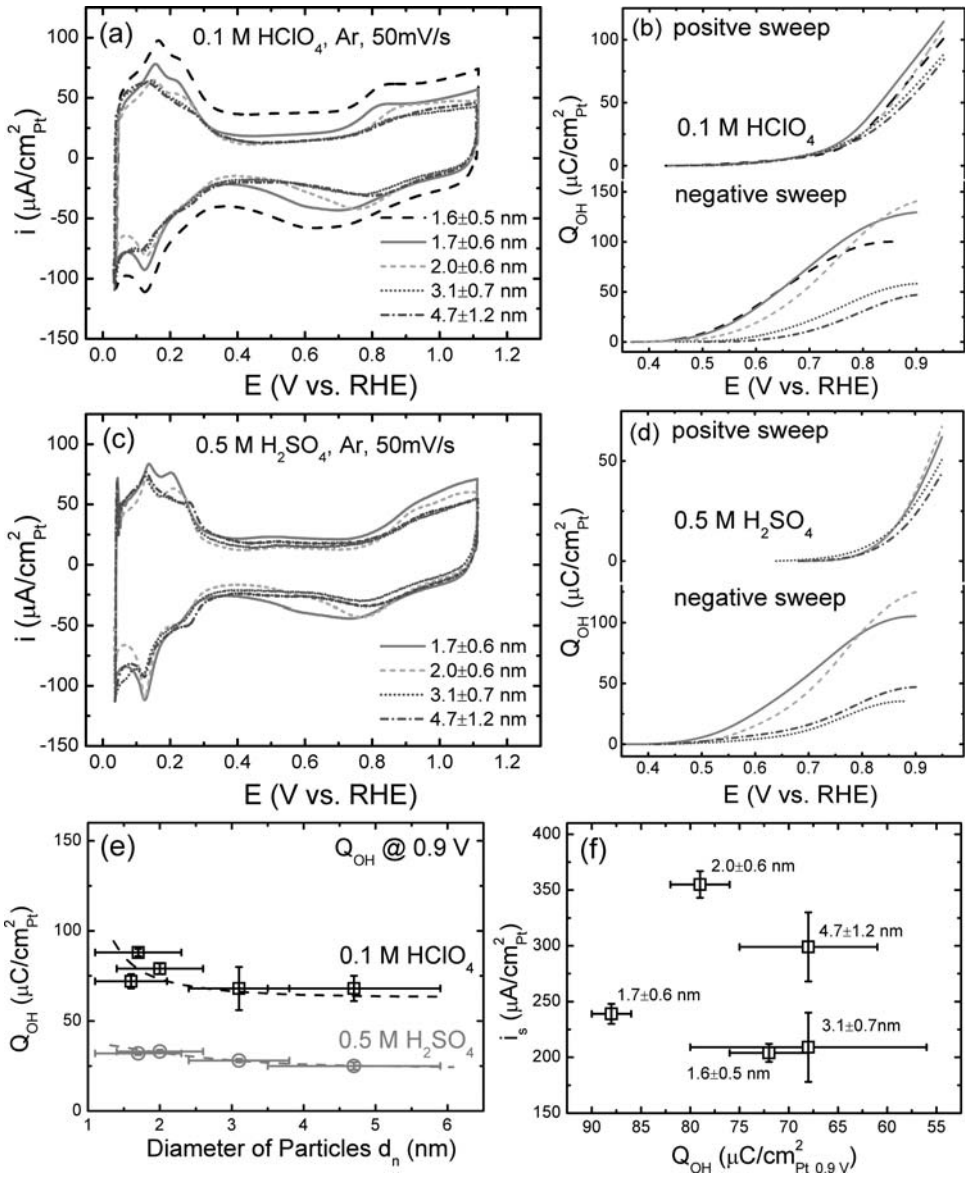

Figure 4. CVs of Pt NPs recorded at room temperature and at a sweep rate of 50 mV/s in (a): 0.1 M Ar-saturated $HClO_4$; and (c): 0.5 M Ar-saturated H_2SO_4. (b): background-corrected charge density associated with Pt-OH formation in the positive sweeps (top) and Pt-OH reduction in the negative sweeps (bottom) in $HClO_4$; (d): background-corrected charge density associated with Pt-OH formation (top) and Pt-OH reduction (bottom) in H_2SO_4; (e): OH coverage at 0.9 V vs. RHE on the positive sweeps in $HClO_4$ and H_2SO_4; and (f): ORR specific activity in HClO4 versus OH coverage at 0.9 V vs. RHE in $HClO_4$. Error bars of the ORR activity are standard deviations constructed from at least four repeats of experiments.

presence of highly oxyphilic Pt clusters in the pristine catalysts, and the formation of more irreversible oxide species.[46]

Size-independent ORR activity.— Representative background-corrected polarization curves of the Pt-46% sample at different rotating speeds in $HClO_4$ and H_2SO_4 are shown in Figures 5a and 5c, respectively. ORR polarization curves of all catalyst samples on RDE show a diffusion-controlled region at voltages lower than 0.6−0.7 V, a diffusion-kinetic combined region, and a kinetic-controlled region[3,10] at voltages equal to or greater than 0.9 V vs. RHE. Background-corrected, diffusion-controlled current densities are well defined for all catalysts as diffusion current densities of different catalysts are very comparable at 1600 rpm and within 5% deviation from the expected limiting current density of ORR in 0.1 M $HClO_4$ at 1600 rpm (6.02 $mAcm^{-2}{}_{disk}$),[47] as shown in Figures 5b and 5d. Representative Koutecky-Levich plots in Figures 5a and 5c insets show that diffusion currents linearly scale with $\omega^{-1/2}$, having Bc_0 parameters of 0.156 $mAcm^{-2}{}_{disk}rpm^{-1/2}$ (obtained at 0.6 V in $HClO_4$) and 0.133 $mAcm^{-2}{}_{disk}rpm^{-1/2}$ (obtained at 0.4 V in H_2SO_4), which is in good agreement with previous studies.[10,47,48] Specific ORR activity i_s is plotted as a function of potential in Figures 5b and 5d insets. It should also be noted that all the catalysts show very similar Tafel slopes of ∼72 mV/dec for $HClO_4$ and 80 mV/dec for H_2SO_4, which agree well with previous studies.[3,48] Interestingly, there is no apparent trend for size-dependent ORR activity, which will be compared and discussed with previous findings[1,10] in detail below.

The specific ORR activity i_s values at 0.9 V vs. RHE in $HClO_4$ and H_2SO_4 of all Pt NP catalysts are compared in Table I and Figure 6a. The specific ORR activity values for all catalyst samples were found to be ∼300 $\mu A/cm^2{}_{Pt}$ in $HClO_4$ and ∼ 60 $\mu A/cm^2{}_{Pt}$ in H_2SO_4, which is in reasonable agreement with those reported previously.[1,3,9,10,49] The five-fold reduction in the specific ORR activity in H_2SO_4 can be attributed to strong adsorption of (bi)sulfate ions as shown previously.[8]

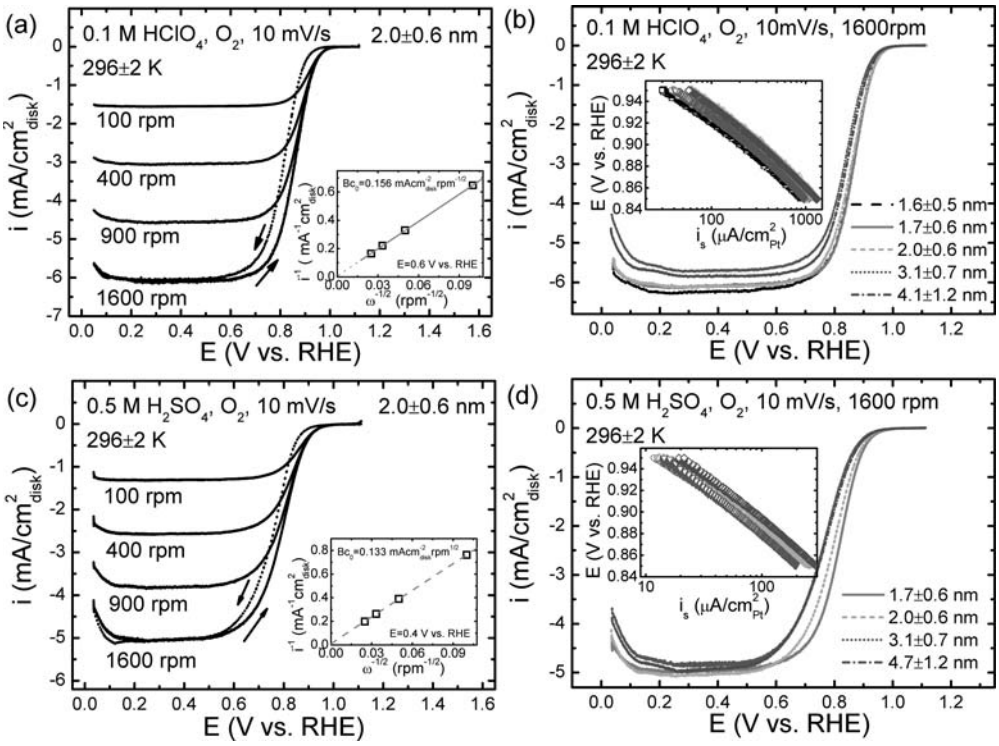

Figure 5. Representative background-corrected polarization curves of ORR on Pt-46% (2.0 ± 0.6 nm) collected at a sweep rate of 10 mV/s and at room temperature in (a): O_2-saturated 0.1 M $HClO_4$ and (c): O_2-saturated 0.5 M H_2SO_4. The rotation rates are 100, 400, 900 and 1600 rpm. Solid lines represent positive-going scans and only negative-going scans at 1600 rpm are shown by the dotted lines. The insets are the Koutecky-Levich plot based on $1/i = 1/i_k + 1/i_D = 1/i_k + 1/Bc_0\omega^{1/2}$ at 0.6 V for $HClO_4$ and 0.4 V for H_2SO_4 vs. RHE; background-corrected polarization curves of ORR on the Pt NPs at a sweep rate of 10 mV/s and at 1600 rpm in (b): O_2-saturated 0.1 M $HClO_4$ and (d): O_2-saturated 0.5 M H_2SO_4. The insets are the Tafel plots of these samples obtained from the normalized polarization curves in the positive-going scans at 1600 rpm. Pt loading of 14 $\mu g_{Pt}/cm^2$on GCE was used for 4.7 ± 1.2 sample, and Pt loading of ~6.4−7.4 $\mu g_{Pt}/cm^2$were used for all the other samples.

As there are a number of previous studies reporting size-dependent ORR activity for Pt NPs, Figure 6b compares the specific ORR activity in 0.1 M $HClO_4$ in this work with those in two landmark studies.[1,10] The specific ORR activity is plotted against the specific ESA of Pt catalysts instead of particle size as different catalysts with comparable sizes of Pt NPs can have very different specific ESA values. The specific ORR activity values at 25 °C from Gasteiger et al.[1] were extrapolated using an activation energy of 10 kJ/mol reported previously.[50] The specific ORR activity on bulk Pt (polycrystalline, pc) having specific ESA close to 0 m^2/g_{Pt} was also included in the plot, which agrees very well with previous reports.[1,10] Significant reduction in the specific ORR activity from over one thousand $\mu A/cm^2{}_{Pt}$on Pt (pc) to several hundreds of $\mu A/cm^2{}_{Pt}$ on Pt/C appears to occur between ~30 m^2/g_{Pt} (~5 nm) and ~10 m^2/g_{Pt} (~15 nm), which is in good agreement with the fact that Pt black (10 ~ 20 nm)[1] or nanostructured thin films of Pt (30 nm)[10] have specific ORR activity approaching that of Pt (pc). Interestingly, we note that the ORR activity values of all Pt/C catalysts scatter from 100 $\mu A/cm^2{}_{Pt}$ to 400 $\mu A/cm^2{}_{Pt}$ without an obvious trend in the ESA range from 30 m^2/g_{Pt} (~5 nm) to 150 m^2/g_{Pt} (~1.5 nm), as shown in Figure 6b. It should be pointed out that the specific ORR activity values of the three pristine Pt/C samples decrease with decreasing particle sizes of Pt NPs (1.6 ± 0.5 nm, 1.7 ± 0.6 nm and 2.0 ± 0.6 nm), which is in agreement with previous findings of similar catalysts with comparable sizes from the same catalyst supplier[10] albeit a much weaker trend in this study. On the other hand, Pt NPs with considerably greater sizes (such as 4.7 ± 1.2 nm) prepared by heat-treatment, do not show higher specific ORR activity. These results suggest that there is no pronounced size influence on the specific ORR activity, which is agreement with previous findings that surface steps on Pt NPs do not reduce the ORR activity significantly.[2] Our previous work[2] has suggested that majority terrace sites instead of minor under-coordinated sites (such as edge and corner sites) on Pt NPs govern specific ORR activity. It is thus postulated that the size-independent activity in particle sizes lower than ~5 nm can be attributed to that the specific ORR activity on majority terrace sites is much greater than those of minority under-coordinated sites. One point of caution

Table I. The number and volume/area averaged diameters ($d_n/d_{v/a}$) over 200 Pt NP counts from HRTEM measurements for each sample, the specific ORR activities and mass activities of Pt NPs in 0.1 M $HClO_4$ and 0.5 M H_2SO_4. The error bars are standard deviations constructed from at least four repeats of measurements for each sample.

	Particle size d_n(nm)/$d_{v/a}$ (nm)	$i_{s,\,0.9V}$ ($\mu A/cm^2{}_{Pt}$) (0.1 M $HClO_4$)	$i_{m,\,0.9V}$ (A/mg_{Pt}) (0.1 M $HClO_4$)	$i_{s,\,0.9V}$ ($\mu A/cm^2{}_{Pt}$) (0.5 M H_2SO_4)	$i_{m,\,0.9V}$ (A/mg_{Pt}) (0.5 M H_2SO_4)
Pt-9%	1.6/2.0	204 ± 8	0.30 ± 0.02		
Pt-19%	1.7/2.2	239 ± 9	0.30 ± 0.01	57 ± 4	0.067 ± 0.004
Pt-46%	2.0/2.4	355 ± 12	0.28 ± 0.01	66 ± 2	0.048 ± 0.002
Pt-46%-900 °C-1m	3.1/3.4	209 ± 31	0.08 ± 0.02	57 ± 6	0.026 ± 0.003
Pt-46%-900 °C-2h	4.7/5.3	299 ± 31	0.07 ± 0.02	72 ± 8	0.017 ± 0.002

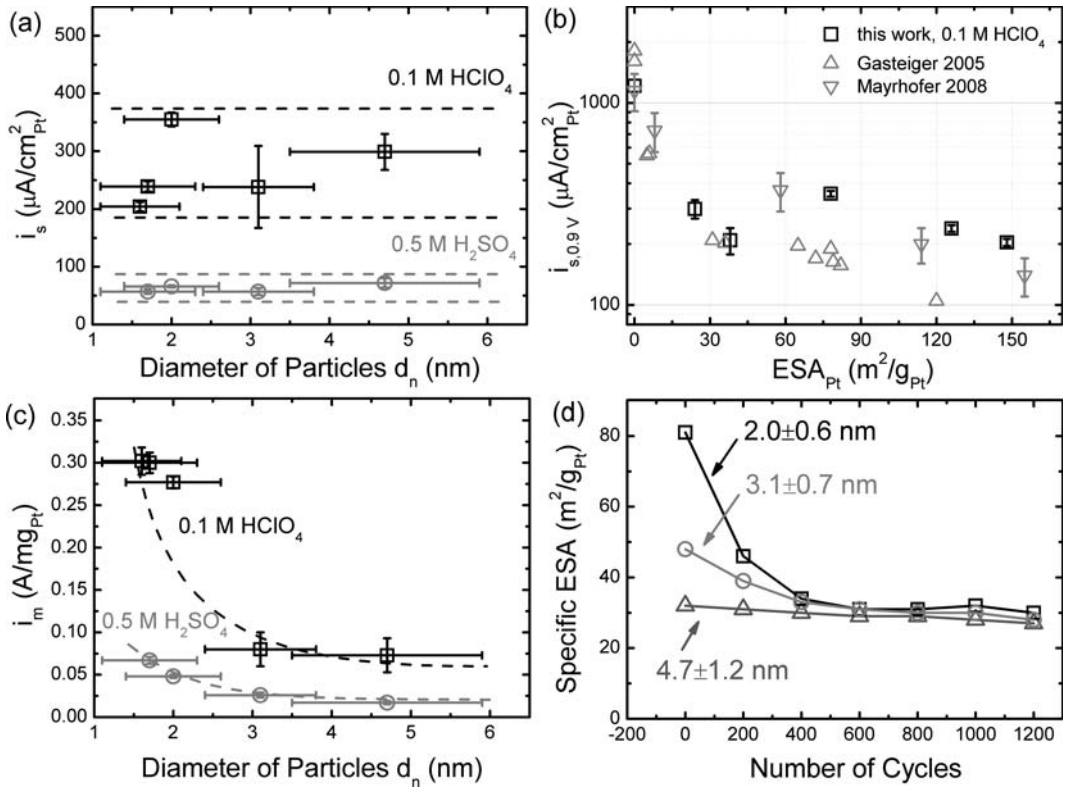

Figure 6. (a): The ORR specific activities at 0.9 V vs. RHE in 0.1 M $HClO_4$ and 0.5 M H_2SO_4as a function of the number-averaged diameter of Pt NPs (d_n); (b): the ORR specific activities at 0.9 V vs. RHE in 0.1 M $HClO_4$ in this work, compared with reference[1] and reference[10] as a function of ESA. Note that the data at 25 °C of Gasteiger 2005 were calculated from the original data in reference[1] at 60 °C using an activation energy of 10 kJ/mol for the ORR as in reference;[50] (c): the ORR mass activities at 0.9 V vs. RHE in 0.1 M $HClO_4$ and 0.5 M H_2SO_4as a function of the number-averaged diameter of Pt NPs (d_n); and (d): The specific ESA of Pt NPs as a function of the number of potential cycles for Pt-46% (2.0 ± 0.6 nm, black squares), Pt-46%-900 °C-1m (3.1 ± 0.7 nm, red circles), and Pt-46%-900 °C-2h (4.7 ± 1.2 nm, blue triangles).

is that the lack of measureable size-dependent ORR activity in this study could be in part due to the use of commercial Pt NPs similar to many previous studies,[1,9,10] where particle size distribution overlap.

As expected from the size-independent specific activity up to ~5 nm, the increased surface area per weight with decreasing sizes dominates the mass activities. As shown in Figure 6c, the mass activities increase with decreasing particle size and reach a maximum for catalysts of 1.6 ± 0.5 nm and 1.7 ± 0.6 nm in $HClO_4$ and H_2SO_4. Specifically, with a three-fold reduction in the number-averaged particle size, the mass activity was found to increase by four-fold from 0.07 A/mg_{Pt} (4.7 ± 1.2 nm) to 0.3 A/mg_{Pt} (1.6 ± 0.5 nm), which agrees reasonably well with the mass activity in the two landmark studies,[1,10] as shown in Figure S4.

Previous work[9] has proposed that the reduced ORR activity with decreasing Pt NP sizes extracted from the positive-going scans can be attributed to increasing coverage of surface oxygenated species (blocking active sites for ORR) on Pt NPs obtained from CV data in the negative-going scans. We reexamine the hypothesis here. Considering that 1) the coverage of oxygenated species in the negative-going scans can differ significantly from that in the positive-going scans at the same potential as shown in Figures 4b and 4d, and 2) there is a considerable difference in the specific activity between the negative-going and positive-going scans, one may argue that it is more appropriate to relate specific ORR activity to the coverage of oxygenated species in the same sweep direction. In comparison to the negative-going sweep, there is a much weaker size-dependence for the coverage of oxygenated species derived from CV in the positive-going sweep, which is in good agreement with the weak size-dependent Pt oxidation as revealed by XPS (Figure 2b), as shown in Figure S5. It is postulated that the presence of very small Pt clusters (smaller than ~0.5 nm, typically not revealed in the conventional HRTEM) in the pristine catalysts, may contribute to the increased Pt oxidation relative to heat-treated catalysts, and thus may give rise to the apparent, very weak size-dependence in CV, XPS, and UPS measurements. However, there is no apparent trend between the ORR activity and the coverage of oxygenated species from CV or the degree of Pt oxidation from XPS measurements, as shown in Figure 4f and Figure S5, respectively. This is consistent with the ORR measurements and NMR results of similar catalysts from the same supplier reported previously.[14] It is proposed that the apparent weak size-dependent ORR activities of three pristine samples found in this study and a stronger size dependence in previous work could result from the fact that not all the ESA measured in the H UPD regions are active for ORR. For example, the surface area of very small Pt NPs (<0.5 nm) and clusters (not considered in the size estimation from conventional TEM) might contribute to ESA but not active for ORR, which can lead to reduced specific ORR activities for Pt-9%. As one may expect that the fraction of these very small Pt NPs and clusters decrease from Pt-9%, Pt-19% to Pt-46%, their contribution to ESA reduces, which can give rise to an apparent size-dependent ORR activity found.

Size-dependent stability upon potential cycling.— Unlike the size-independent ORR activity, the instability of Pt NPs was strongly dependent on the particle size even in the narrow size range, as shown in Figure 6d and Figure S6. Upon potential cycling, Pt NPs with Pt-46% (2.0 ± 0.6 nm) exhibit a faster current drop in the Pt-H interaction than Pt-46%-900 °C-2h (4.7 ± 1.2 nm), and in the Pt-OH region, as shown in Figures S6a and S6b, respectively. The specific ESA of Pt NPs of 2.0, 3.1 and 4.7 nm is plotted as a function of the number of potential cycles in Figure 6d, where the fraction of ESA loss decreases with increasing particle sizes. The ESA loss of Pt NPs of 2.0 nm upon potential cycling was accompanied with the growth of Pt NPs, where

the number of particles below 1 nm decreased considerably after 1200 cycles. On the other hand, no visible change was detected for Pt NPs of 4.7 nm before and after cycling as shown in Figure S7.

Previous studies[5,19,23,25] have shown that the size-dependent stability can be explained reasonably well by curvature effects as described by the Gibbs-Thomson relation. Upon voltage cycling, oxygenated species on under-coordinated sites on Pt NPs and clusters can dissolve, which leads to loss of Pt mass (soluble Pt species) into the acid solution, and deposition of soluble Pt species onto larger Pt NPs upon potential cycling to lower potentials (Ostwald-ripening). Smaller particles with greater fractions of under-coordinated sites can show higher oxyphilicity towards O-containing species, and pristine Pt-46% may contain small clusters that might not be detectable by HRTEM as mentioned above. Therefore, it is hypothesized that the ESA loss for Pt NPs of 2 nm (pristine Pt-46%) could come from Pt dissolution of smaller particles (smaller than 1 nm), and Ostwald ripening by which particles grow at the expense of smaller particles.

Conclusions

We have demonstrated that there is no pronounced size influence on the specific ORR activity on HSAC-supported Pt NPs between ~1 nm and ~5 nm in both $HClO_4$ and H_2SO_4. This is in agreement with the size-independent OH anion coverage obtained from CV measurements from the same sweep direction. In addition, although XPS and UPS measurements reveal that the Pt oxides and the surface valence band structure of Pt NPs below 5 nm are weakly dependent on the particle size, this slight dependence are not sufficient to cause observable size-dependence of the ORR activity beyond experimental uncertainty. Our study suggests that TEM measured "particle size" is not accurate to describe ORR behavior of different sized Pt NPs obtained from TKK due to the TEM detection limit on extremely small particles (<0.5 nm). It is therefore suggested that ESA should be used to describe the so-called "size effect" on NPs as it better reflects the particle size and size distribution. In contrast, the instability of Pt NPs in acidic environment is found to strongly depend on the particle size. Only one-nanometer increase in the particle diameter can substantially stabilize Pt NPs under simulated PEMFC operation conditions. It suggests that a balance has to be maintained in terms of decreasing particle sizes to obtain larger surface areas, thus a better overall PEMFC performance while keeping a reasonable lifetime of the catalysts under PEMFC operation.

Acknowledgment

The authors would like to thank Ethan J. Crumlin for XPS measurements and Prof. Dane Morgan (Materials Science and Engineering, University of Wisconsin, Madison) for discussion. This work was supported in part by the DOE Hydrogen Initiative program under award number DE-FG02-05ER15728. This research made use of the Shared Experimental Facilities supported by the MRSEC Program of the National Science Foundation under award number DMR 02-13282. The National Synchrotron Light Source, Brookhaven National Laboratory, is supported by the U.S. Department of Energy, Office of Science, Office of Basic Energy Sciences, under Contract No. DE-AC02-98CH10886.

References

1. H. A. Gasteiger, S. S. Kocha, B. Sompalli, and F. T. Wagner, *Applied Catalysis B-Environmental*, **56**, 9 (2005).
2. S. W. Lee, S. Chen, J. Suntivich, K. Sasaki, R. R. Adzic, and Y. Shao-Horn, *Journal of Physical Chemistry Letters*, **1**, 1316 (2010).
3. U. A. Paulus, T. J. Schmidt, H. A. Gasteiger, and R. J. Behm, *Journal of Electroanalytical Chemistry*, **495**, 134 (2001).
4. P. J. Ferreira, G. J. la O', Y. Shao-Horn, D. Morgan, R. Makharia, S. Kocha, and H. A. Gasteiger, *Journal of the Electrochemical Society*, **152**, A2256 (2005).
5. Y. Shao-Horn, W. C. Sheng, S. Chen, P. J. Ferreira, E. F. Holby, and D. Morgan, *Topics in Catalysis*, **46**, 285 (2007).
6. V. R. Stamenkovic, B. Fowler, B. S. Mun, G. F. Wang, P. N. Ross, C. A. Lucas, and N. M. Markovic, *Science*, **315**, 493 (2007).
7. K. Kinoshita, *Journal of the Electrochemical Society*, **137**, 845 (1990).
8. N. M. Markovic and P. N. Ross, *Surface Science Reports*, **45**, 121 (2002).
9. K. J. J. Mayrhofer, B. B. Blizanac, M. Arenz, V. R. Stamenkovic, P. N. Ross, and N. M. Markovic, *Journal of Physical Chemistry B*, **109**, 14433 (2005).
10. K. J. J. Mayrhofer, D. Strmcnik, B. B. Blizanac, V. Stamenkovic, M. Arenz, and N. M. Markovic, *Electrochimica Acta*, **53**, 3181 (2008).
11. D. S. Strmcnik, P. Rebec, M. Gaberscek, D. Tripkovic, V. Stamenkovic, C. Lucas, and N. M. Markovic, *Journal of Physical Chemistry C*, **111**, 18672 (2007).
12. Y. Takasu, N. Ohashi, X. G. Zhang, Y. Murakami, H. Minagawa, S. Sato, and K. Yahikozawa, *Electrochimica Acta*, **41**, 2595 (1996).
13. S. Mukerjee and J. McBreen, *Journal of Electroanalytical Chemistry*, **448**, 163 (1998).
14. H. Yano, J. Inukai, H. Uchida, M. Watanabe, P. K. Babu, T. Kobayashi, J. H. Chung, E. Oldfield, and A. Wieckowski, *Physical Chemistry Chemical Physics*, **8**, 4932 (2006).
15. M. Peuckert, T. Yoneda, R. A. D. Betta, and M. Boudart, *Journal of the Electrochemical Society*, **133**, 944 (1986).
16. G. A. Tritsaris, J. Greeley, J. Rossmeisl, and J. K. Norskov, *Catalysis Letters*, **141**, 909 (2011).
17. T. Akita, A. Taniguchi, J. Maekawa, Z. Sirorna, K. Tanaka, M. Kohyama, and K. Yasuda, *Journal of Power Sources*, **159**, 461 (2006).
18. R. Borup, J. Meyers, B. Pivovar, Y. S. Kim, R. Mukundan, N. Garland, D. Myers, M. Wilson, F. Garzon, D. Wood, P. Zelenay, K. More, K. Stroh, T. Zawodzinski, J. Boncella, J. E. McGrath, M. Inaba, K. Miyatake, M. Hori, K. Ota, Z. Ogumi, S. Miyata, A. Nishikata, Z. Siroma, Y. Uchimoto, K. Yasuda, K. I. Kimijima, and N. Iwashita, *Chemical Reviews*, **107**, 3904 (2007).
19. E. F. Holby, W. C. Sheng, Y. Shao-Horn, and D. Morgan, *Energy & Environmental Science*, **2**, 865 (2009).
20. K. Yasuda, A. Taniguchi, T. Akita, T. Ioroi, and Z. Siroma, *Physical Chemistry Chemical Physics*, **8**, 746 (2006).
21. Z. W. Chen, M. Waje, W. Z. Li, and Y. S. Yan, *Angewandte Chemie-International Edition*, **46**, 4060 (2007).
22. M. K. Debe, A. K. Schmoeckel, G. D. Vernstrorn, and R. Atanasoski, *Journal of Power Sources*, **161**, 1002 (2006).
23. L. Tang, B. Han, K. Persson, C. Friesen, T. He, K. Sieradzki, and G. Ceder, *Journal of the American Chemical Society*, **132**, 596 (2010).
24. K. Yasuda, A. Taniguchi, T. Akita, T. Ioroi, and Z. Siroma, *Journal of the Electrochemical Society*, **153**, A1599 (2006).
25. R. M. Darling and J. P. Meyers, *Journal of the Electrochemical Society*, **150**, A1523 (2003).
26. J. J. Yeh and I. Lindau, *Atomic Data and Nuclear Data Tables*, **32**, 1 (1985).
27. B. S. Mun, M. Watanabe, M. Rossi, V. Stamenkovic, N. M. Markovic, and P. N. Ross, *Journal of Chemical Physics*, **123**, 204717 (2005).
28. W. Eberhardt, P. Fayet, D. M. Cox, Z. Fu, A. Kaldor, R. Sherwood, and D. Sondericker, *Physical Review Letters*, **64**, 780 (1990).
29. S. W. Lee, B. S. Kim, S. Chen, Y. Shao-Horn, and P. T. Hammond, *Journal of the American Chemical Society*, **131**, 671 (2009).
30. J. L. G. de la Fuente, S. Rojas, M. V. Martinez-Huerta, P. Terreros, M. A. Pena, and J. L. G. Fierro, *Carbon*, **44**, 1919 (2006).
31. S. Wang, S. P. Jiang, T. J. White, J. Guo, and X. Wang, *J. Phys. Chem. C*, **113**(43), 18935 (2009).
32. S. Chen, W. C. Sheng, N. Yabuuchi, P. J. Ferreira, L. F. Allard, and Y. Shao-Horn, *Journal of Physical Chemistry C*, **113**, 1109 (2009).
33. F. C. Nart and W. Vielstich, in *Handbook of Fuel Cells − Fundamentals, Technology and Applications*, H. A. G. a. A. L. Wolf Vielstich Editor, p. 302, John Wiley & Sons, Ltd. (2003).
34. A. J. Bard and L. R. Faulkner, *Electrochemical Methods: Fundamentals and Applications*, John wiley & Sons, New York (2001).
35. K. A. Cherian, S. D. Wolter, and R. Roy, *Diam Relat Mater*, **6**, 1747 (1997).
36. E. Lewin, K. Buchholt, J. Lu, L. Hultman, A. L. Spetz, and U. Jansson, *Thin Solid Films*, **518**, 5104 (2010).
37. B. C. Han, C. R. Miranda, and G. Ceder, *Physical Review B*, **77**, 075410 (2008).
38. V. Murgai, S. Raaen, M. Strongin, and R. F. Garrett, *Physical Review B*, **33**, 4345 (1986).
39. S. Raaen and M. Strongin, *Physical Review B*, **32**, 4289 (1985).
40. B. Hammer, O. H. Nielsen, and J. K. Norskov, *Catalysis Letters*, **46**, 31 (1997).
41. J. K. Norskov, *Reports on Progress in Physics*, **53**, 1253 (1990).
42. Y. Sun, L. Zhuang, J. Lu, X. Hong, and P. Liu, *Journal of the American Chemical Society*, **129**, 15465 (2007).
43. M. Lynch and P. Hu, *Surface Science*, **458**, 1 (2000).
44. S. W. Lee, S. Chen, W. C. Sheng, N. Yabuuchi, Y. T. Kim, T. Mitani, E. Vescovo, and Y. Shao-Horn, *Journal of the American Chemical Society*, **131**, 15669 (2009).
45. J. Zhang, K. Sasaki, E. Sutter, and R. R. Adzic, *Science*, **315**, 220 (2007).
46. H. Angerste, B. E. Conway, and W. B. A. Sharp, *Journal of Electroanalytical Chemistry*, **43**, 9 (1973).
47. N. M. Markovic, H. A. Gasteiger, and P. N. Ross, *Journal of Physical Chemistry*, **99**, 3411 (1995).
48. U. A. Paulus, A. Wokaun, G. G. Scherer, T. J. Schmidt, V. Stamenkovic, V. Radmilovic, N. M. Markovic, and P. N. Ross, *Journal of Physical Chemistry B*, **106**, 4181 (2002).
49. D. van der Vliet, D. S. Strmcnik, C. Wang, V. R. Stamenkovic, N. M. Markovic, and M. T. M. Koper, *Journal of Electroanalytical Chemistry*, **647**, 29 (2010).
50. K. C. Neyerlin, W. B. Gu, J. Jorne, and H. A. Gasteiger, *Journal of the Electrochemical Society*, **153**, A1955 (2006).